Preparation and Characterization of Cr-free passivation films on zinc coating using Response Surface Methodology and Electrochemical Methods

Yuhan Yao, Zhaolin Zhan, Jianxiong Liu, Xiao Wang, Xiaohua Yu, Ju Rong**

Faculty of Materials and Engineering, Kunming University of Science and Technology, Kunming, Yunnan 650093, P. R. China
*E-mail: JRong_kmust@163.com (Rong Ju), and xiaohua_y@163.com (Yu Xiaohua)

Response surface methodology (RSM) was used in this study to determine the optimum operating conditions for the reduction of galvanized sheet corrosion using a Cr-free passivation films. Passivation films layer with strong corrosion resistance was formed on the surface of galvanizing which was impregnated in chromium-free passivating agent. Furthermore, the RSM was used to ascertain the main and interactive effects (deviation between the experimental and theoretical values: 0.12%). The coefficient of determination (R^2) showed that the RSM approach was appropriate for optimization of the Cr-free passivator. Silane coupling agent, ammonium molybdate, nanosilica, and tannic acid played a key role in changing the corrosion area and potential. The results revealed that, compared with Cr^{6+} passivation, Cr-free passivation yielded considerably more homogeneous and smoother surfaces (surface roughness of Cr-free passivation film: 0.54 μm). In addition, the properties of the zinc coating after Cr-free passivation were clearly superior to those of the zinc coating subjected to the conventional Cr^{6+} passivation treatment. E_{corr}, current density, and polarization resistance values of this superior coating were -1073 mV, 0.017 A cm^{-2}, and 989.2 Ω, respectively. This study can serve as an experimental and a theoretical guide for the development of Cr-free passivation films.

Keywords: Cr-free passivation film; galvanized sheet; electrochemical corrosion

1. INTRODUCTION

Owing to the poor corrosion resistance of iron, zinc coatings are commonly plated (via hot-dip galvanizing or galvanizing) to enhance the robustness of plain steels through barrier protection and sacrificial protection [1–3]. Nevertheless, due to the presence of highly carcinogenic Cr6+ compounds during the passivation treatment, these coatings is strongly restricted to use, the toxicity of hexavalent chromium is common currency. Exposing to the substance on long-term basis is more likely to develop

lung cancer, in accordance with international regulations such as RoHS and WEEE [4, 5]. Therefore, methods for improving Cr-free passive films have attracted significant attention [6, 7]. Despite extensive research focused on other types of metal salts for replacing hexavalent chromium as passivation for hot-dip galvanized steel (HDG), there still does not exist any less reasonable formula.

In recent years, many Cr-free passivation experiments, for e.g., molybdate [8], titanium [9], silicate [10], and phosphate passivation [11], have been performed. A passive film on electrogalvanized steel prevents contacting between the metal substrate and the corrosive environment, thereby protecting the substrate from corrosion attack. According to GangKong [12], a molybdate passivation film and a galvanized sheet can synergistically inhibit the occurrence of corrosion. A combination treatment of molybdate salts and silane on galvanized steel yields excellent corrosion resistance and self-repairing capability [13]. However, in most cases, the corrosion resistance of the Cr-free passivation films is lower than that of the conventional Cr^{6+} passivation films [14, 15].

The corrosion reaction is affected by several factors, and the influence exerted by different proportions of the passivating agent on the corrosion performance, which is difficult to determine [17]. Response surface methodology (RSM) represents a combination of mathematical and statistical methods applied to the experiential modeling and analysis of several input data [18], which may influence the results or quality characteristics of the process. RSM has been widely used in many corrosion fields, such as microbial corrosion [19], electrochemistry [20], and material design [21]. In the present study, a Cr-free passivation films are important to obtain an optimized metered passivator that exhibits excellent corrosion resistance. This, to the best of our knowledge, represents the first-ever application of RSM to the optimization of Cr-free passivation.

This work proposes an RSM method to design a metering ratio of a Cr-free passivation agent. A Cr-free composite passivator is prepared by tannic acid, organosilane, ammonium molybdate, and nanosilica. The chemical compositions and microstructures of the films are assessed by scanning electron microscopy (SEM), X-ray photoelectron spectroscopy (XPS), and by using an electrochemical workstation.

2. MATERIALS AND METHODS

2.1 Materials and preparation

The following chemicals were employed in this study: silane coupling agent (KH151 $(OCH_2CH_3)_3$, Nanjing Shuguang Chemical Factory); trivalent chromium passivation agent (439ET, Nanjing Shuguang Chemical Factory); ammonium molybdate $(H_{24}Mo_7N_6O_{24} \cdot 4H_2O$, AR, Aladdin); tannic acid $(C_{76}H_{52}O_{46}$, AR, Aladdin); nanosilica (100–200 nm, Aladdin); NaCl (99.96%, Aladdin); and galvanized steel (Dx51d, Anshansteel).

The Cr-free passivator was prepared by the following steps: i) dissolve silane coupling agent liquid (4.0 wt.%) into 500 mL of deionized water; ii) add ammonium molybdate (1.55 wt.%), tannic acid (3.15 wt.%), and nanosilica (3.53 wt.%) to the solution; iii) leave the solution undisturbed for 24 h in a vacuum incubator at 25ºC.

The Cr^{6+} passivation film (S1) was prepared by the following steps: i) degrease and pickle the galvanized steel (600 mm×100 mm×0.5 mm); ii) place the cleaned sheet in a dry box (120°C, 1 h); iii) perform passivation by dip-coating the sheet in a trivalent chromium passivation agent (room temperature, 30 s).

The Cr-free passivation film (S2) was prepared by the following steps: i) degrease and pickle the galvanized steel (600 mm×100 mm×0.5 mm); ii) place the cleaned sheet in a dry box (120°C, 1 h); and iii) perform passivation by dip-coating the sheet in a Cr-free passivation films (room temperature, 30 s).

2.2 Analysis and testing

The microstructure was characterized by means of a scanning electron microscope (SEM, TESCAN VEGA3) coupled with energy dispersive X-ray spectroscopy (EDS) operated at 5 kV. The phase structure was determined by X-ray diffractometry (XRD, D/Max-2200), operating at 30 kV and 30 mA and employing Cu-K_α radiation ($\lambda = 0.15406$ nm) in the 2θ range 30°–90°. The surface chemical state of the product was analyzed by X-ray photoelectron spectroscopy (XPS, PHI5000 Versaprobe-II ULVAC-PHI) employing Al-Kα radiation. The MATLAB software was used to carry on binarization processing for pre-processed grayscale images. The MIAPS multifunctional image processing software was employed to extract the distribution the area ratio of the corrosion pit from the binary images.

The electrochemical behavior of S1 and S2 was investigated by means of corrosion potential (E_{corr}) and potentiodynamic polarization measurements. Electrochemical measurements were carried out by a CHI 760E electrochemical workstation. Potentiodynamic polarization measurements were recorded in 0.05 M NaCl aqueous solution using a standard three-electrode setup with a platinum plate, saturated calomel electrode (SCE), and zinc coating after different passivation treatments. The area of the working electrode was 3.6 cm^2, the scan rate was 0.2 mV/s. The working electrode was immersed in 0.05 M NaCl aqueous solution for 30 min and a stable open circuit potential (OCP) was then established by applying a current. Potentiodynamic polarization curves were obtained by varying the electrode potential from -1.5 V to +1.5 V around the OCP against SCE. The corrosion resistance of the S1 and S2 was evaluated by means of electrochemical impedance spectroscopy (EIS) in 0.5 M NaCl solution. Impedance measurements were carried out at open circuit potential with AC voltage amplitude of 50 mV and frequency range from 10 mHz to 100 kHz. EIS measurements were recorded using a conventional three-electrode setup with a platinum plate, SCE, and zinc coating after different passivation treatments. The area of the working electrode was 3.6 cm^2 also for impedance measurements.

2.3 Design of experiments and statistical analysis

The Plackett–Burman Design (PBD) is an efficient screening method for identifying the important factors (among a large number of factors) that influence a process. For the corrosion area and potential, significant variables, such as silane coupling agent (A), ammonium molybdate (B), nanosilica (C), tannic acid (D), H_2TiF_6 (E), $AlH_2(PO_4)_3$ (F), and phytic acid (G) were chosen as the independent variables and blank controls were referred to as H–K. For mathematical modeling, the following first-order polynomial model

was used (Eq. 1) [22].

$$Y=\beta_0+\sum\beta_i x_i \tag{1}$$

where Y is the predicted response (corrosion area and potential), β_0 is the model intercept, β_i is the linear coefficient, and x_i is the level of the independent variable. The experimental design of PBD (factors and tested range) is shown in Table 1.

Table 1. Plackett–Burman Design of factors

run order	A	B	C	D	E	F	G	H	I	J	K	corrosion potential (mV)	corrosion area (%)
1	6	2.0	3	2	0	5	0	1	1	-1	1	-1104	0.7
2	2	2.0	6	6	0	2	0	1	-1	1	1	-2156	30.4
3	6	2.0	3	6	1	5	0	-1	-1	1	-1	-1946	13.9
4	6	0.5	6	6	0	5	1	1	-1	-1	-1	-1174	1.9
5	2	2.0	3	6	1	2	1	1	1	-1	-1	-2560	44.4
6	6	0.5	6	6	1	2	0	-1	1	-1	1	-1170	8.5
7	2	0.5	3	2	0	2	0	-1	-1	-1	-1	-1660	18.8
8	2	2.0	6	2	1	5	1	-1	-1	-1	1	-1507	29.7
9	6	2.0	6	2	0	2	1	-1	1	1	-1	-1115	0.2
10	6	0.5	3	2	1	2	1	1	-1	1	1	-1042	2.8
11	2	0.5	6	2	1	5	0	1	1	1	-1	-1276	8.5
12	2	0.5	3	6	0	5	1	-1	1	1	1	-2134	36.9

Four significant factors were selected using PBD. Following that, a factorial Central Composite Design (CCD) and RSM were performed to identify the significant effects and the interactions between the selected factors with a positive influence on the corrosion resistance. The optimal value of each variable that would lead to the maximum anti-corrosion was also identified. In this study, a four-factor, five-level CCD with 20 runs was employed. The four factors were selected from PBD. Furthermore, the four kinds of Cr-free passivation raw material solution with silane coupling agent, ammonium molybdate, nanosilica, and tannic acid were also being optimized. The independent variables were divided into three levels (low, basal, and high) with coded value (−1, 0, +1) and the star points of +2 and −2 for +α and –α, respectively.

3. RESULTS AND DISCUSSION

In this study, silane coupling agent (A), ammonium molybdate (B), nanosilica (C), and tannic acid (D) were the independent variables and the percentage of reduction in corrosion potential (E_1) and area (E_2) were the dependent output response of the system. Each factor was selected from five levels of experimental design. The 30 groups of experiment consisted of eight axis points, 16 factor points, and six center points (shown in Table 2 for the corresponding RSM design factor table). Application of the RSM based on parameter estimates and the experimental results revealed an empirical relationship

between the response and the input variables. This relationship was described by the following fitted regression model, which is expressed as a second-order polynomial equation:

$$E_1=-1.02+0.029A+2.229\times10^{-3}B-0.018C+4.338\times10^{-3}D+2.106AB- \quad\quad (2)$$
$$6.969\times10^{-3}AC-8.269\times10^{-3}AD-0.011BC-1.431\times10^{-3}BD+4.694\times10^{-3}CD-$$
$$0.044A^2-0.060B^2-0.042C^2-0.046D^2 \quad (P<0.0001, R^2=0.9656)$$

$$E_2=12.37+4.78A+1.17B-0.52C+1.68D0.61AB-1.55AC- \quad\quad (3)$$
$$0.075AD+0.013BC+1.49BD-4.28CD+2.06A^2-2.31\ B^2-1.44\ C^2-1.39\ D^2$$
$$(P<0.01, R^2=0.8039)$$

Table 2. RSM design factors

Independent variables	Coded factor level				
	α	-1	0	1	α
A Silane coupling agent	2.0	3.0	4.0	5.0	6.0
B Ammonium molybdate	1.0	1.2	1.5	1.75	2.0
C Nanosilica	3.0	3.5	4.0	4.5	5.0
D Tannins	2.0	3.0	4.0	5.0	6.0

Based on Table 3, the coefficient of determination (R^2) was 0.9656 and 0.8039, indicating a close correlation between the observed and predicted values. In addition, very low probability values of 0.00013 and 0.00091 were obtained. A p-value, which is lower than 0.01, indicated that the model was considered statistically significant [23].

Table 3. Variance and significance analysis

| Source of variance	Corrosion potential (V)			Corrosion area (%)		
	Sum of squares	DF	*P*-value	Sum of squares	DF	*P*-value
Model	0.210	14	0.00013	1433.740	14	0.0036
A	0.020	1	0.00091	549.130	1	0.0002
B	0.193	1	0.6348	33.130	1	0.2518
C	7.403	1	0.0017	6.410	1	0.6079
D	4.515	1	0.03604	68.010	1	0.1083
AB	7.098	1	0.7136	6.000	1	0.6193
AC	7.770	1	0.2349	38.440	1	0.2187
AD	1.094	1	0.1626	0.0900	1	0.9513
BC	1.991	1	0.0662	0.003	1	0.9919
BD	3.278	1	0.8028	35.400	1	0.2369
CD	3.521	1	0.4176	292.410	1	0.0030
A^2	0.052	1	< 0.0001	116.680	1	0.0409
B^2	0.098	1	< 0.0001	146.680	1	0.0241
C^2	0.049	1	< 0.0001	56.680	1	0.0399
D^2	0.057	1	< 0.0001	52.800	1	0.1532
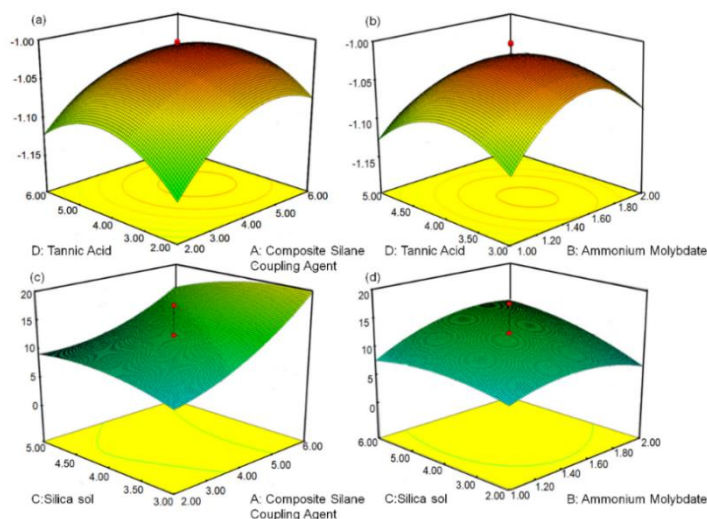
Figure 1. Response surface plot of: (a) silane coupling agent and tannic acid; (b) ammonium molybdate and tannic acid on corrosion potential of Cr-free passivation films; (c) silane coupling agent and nanosilica; (d) ammonium molybdate and nanosilica on corrosion area of Cr-free passivation films.

From Table 3, AD and BC have considerable influence on the corrosion potential, and AC, BD affect the main corrosion area. The effect of AD and BC on the reduction in corrosion potential is depicted in Fig. 1 a-b. The best corrosion potential performance of the passivation film of the Cr-free passivation films was realized at A, B, C, and D contents corresponding to 4.0, 3.1, 1.5, and 3.5 wt.%, respectively. Fig. 1c and d show the effect of AC and BD on the reduction at corrosion area. The best corrosion performance of the film of the passivator was realized at A, B, C, and D contents corresponding to 4.0, 1.5, 3.9, and 3.9 wt.%, respectively.

The corrosion potential and the corrosion area were verified via experiments (corresponding results as shown in Table 4). The results showed that the formulation obtained with the corrosion potential as the response yielded a smaller error than the other formulations. The corrosion potential verification value (-1031 mV) and the corrosion area verification value (4.80%) was close to the corresponding theoretical values (-1077 mV, 4.94%; relative error: 0.12% and 2.21%, respectively).

Table 4. Test results verifying the formulation of the passivator

Index	Predicted Value		Experimental Value	
	Corrosion Potential (mV)	Corrosion Area(%)	Corrosion Potential(mV)	Corrosion Area(%)
Passivation films S2	-1031	4.94	-1077	4.80

3.1 Microstructural and elemental composition

The SEM image and EDS results of S1 (which was mainly composed of C, O, Zn, Si, and P; Fig. 2a) shows many micro-cracks and defects, such as coated zinc particles, zinc bismuth, and scratches.

These defects, which were absent from S2 (Fig. 2b), may break in the corrosive medium, leading to fall off [24]. This absence showed that, owing to the Cr-free passivation film, the original defects on the surface of the galvanized sheet could be eliminated and the surface quality of the sheet could be improved (Fig. 2b). Moreover, the mass percentage of Mo for S2 sample increased to 1.13 wt.%. Therefore, the passivation film on the surface was formed by a Cr-free passivating agent with a high Mo content.

The presence of voids in the passivated films and the smoothing mechanism of the Cr-free passivation layers were explained by means of surface roughness measurements. The roughness value of S2 (0.54–0.90 μm) was lower than that of S1 (0.70–1.30 μm). As shown in Fig. 2 c-d, many defects persist even after the completion of passivation. These results indicated that adding an appropriate Cr-free passivating agent to the galvanized sheet increased the smoothness of the sheet and reduced the number of surface defects in the sheet, indicating a relative high degree of passivation films structure [25].
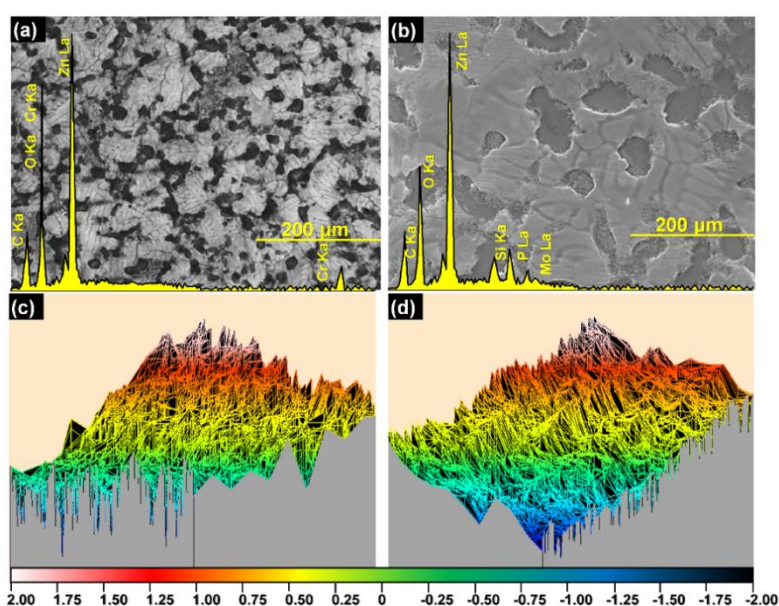

Figure 2. SEM images and EDS of zinc coatings after (a) Cr-free passivation and (b) Cr^{6+} passivation; in addition, (c) Cr^{6+} passivation film and (d) Cr-free passivation film are corresponding to the roughness images.

3.2 Phase composition and valence state of elements

The X-ray diffraction (XRD) patterns of S1 and S2 spheres were characterized by well-defined diffraction peaks distributed over the 2θ range (30 to 90°) in Fig. 3. Peaks (corresponding to Zn) occurred in both sets of samples, indicating that Zn existed in the coating (PDF#04-0831). In addition, broad diffraction peaks were observed at 2θ of ~64.9°, 75.3°, 82.3°, and 86.9°. These corresponded to the MoO_3 (152) peak (PDF#24-1133) and $Mo(OH)_2$ (213), (205), (220) peaks (PDF#16-0687) [26, 27], respectively. The results shown that the passivation film on the surface of S2 was formed mainly from the Cr-free Mo-containing passivation agent.
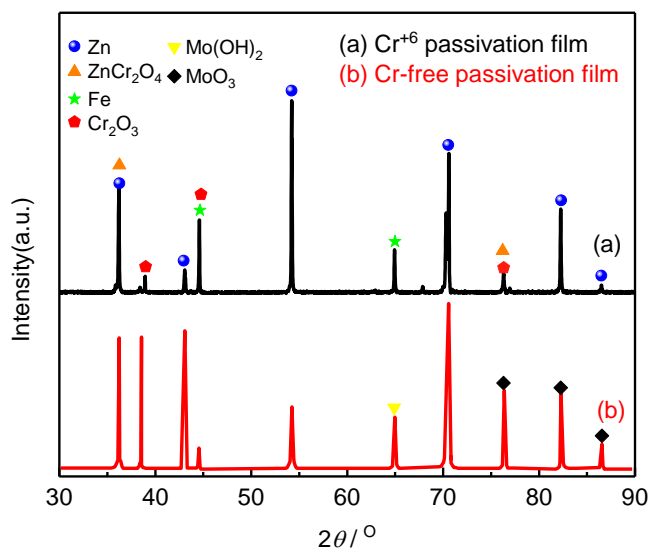
Figure 3. Wide-angle XRD patterns of (a) Cr-free passivation and (b) Cr^{6+} passivation obtained for 2θ ranging from 30° to 90°.

The chemical composition of the composite sample was further investigated via XPS (see Fig. 4 for the corresponding results). The four peaks occurring at 232.6, 233.9, 242.5, and 243.6 eV corresponded to the Mo 3d core-level spectrum, i.e., Mo 3d (see Fig. 4a). Additionally, the O 1s peak at 531.02 eV and the satellite peak at 532.42 eV (Fig. 4b) could be attributed to O^{2-} and OH$^-$ [28], respectively. These results confirmed that the Mo element in S1 sample was successfully introduced into the galvanized sheet, as previously indicated by the XRD results.
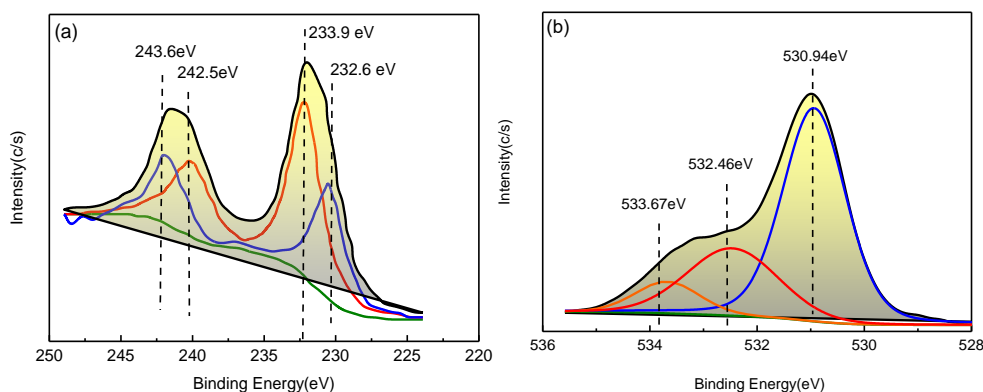

Figure 4. XPS survey spectrum, the corresponding core levels of zinc coatings after Cr-free passivation (a) Mo 3d and (b) O 1s.

3.3 Electrochemical properties

The corrosion resistance of different samples in simulated seawater at room temperature was evaluated via the potentiodynamic polarization technique. Fig. 5 shows the potentiodynamic polarization curves, and Table 5 shows the obtained electrochemical parameters, such as E_{corr}, β_a, β_c, and i_{corr}. As the

table shows, the i_{corr} of the coarse-grained zinc coatings after Cr-free passivation (i_{corr}= 0.017A/cm^2) was significantly lower than that after Cr^{6+}passivation (i_{corr} = 0.223 A/cm^2).
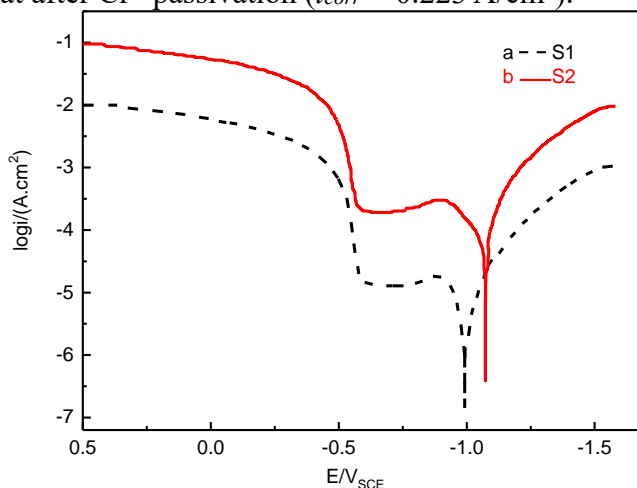

Figure 5. Potentiodynamic polarization curves of zinc coatings after (a) Cr^{6+}passivation and (b) Cr-free passivation in 0.05 M NaCl solution at 25 ± 1 °C.

Table 5. Electrochemical parameters of zinc coating after Cr^{6+} passivation (S1) and Cr-free passivation (S2)

Sample	E_{corr} (mV)	β_a (mV dec^{-1})	j_{corr} (A cm^{-2})
S1	-1173	81.7	0.223
S2	-1031	249.3	0.017

The results obtained from the electrochemical impedance spectroscopy (EIS) experiments performed on S1 and S2 are shown in Fig. 6. As shown in the figure, the Nyquist plots of two electrodes were obtained. Each plot consists of a compressed semicircle and a straight line, which occur at high frequency and low frequency, respectively. The corresponding equivalent circuit is also shown in Fig. 6.
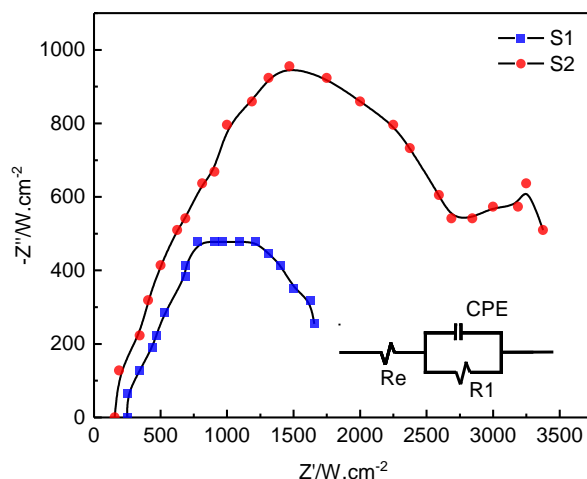

Figure 6. EIS of zinc coating after Cr^{6+}passivation (S1) and Cr-free passivation (S2) at open circuit potential with AC voltage amplitude of 50 mV.

The data are fitted by (shown in Table 6 for the relevant parameters) using the Zsimple software. The parameters R_S, R_{pf}, and R_{po}, corresponding to the solution resistance, first loop of the Nyquist plot, and pore resistance, respectively, were essential for a perfect coating. C_1 is the capacitance of the porous outer layer. The R_s values of S1 and S2 were 871.3 and 989.2 Ω, respectively. Furthermore, the EIS results revealed that the barrier layer resistance of S2 was considerably higher than that of S1. The values of the impedance reflected the ease with which the electrolyte diffused into the pores of the membrane, i.e., the corrosion resistance of the sample increases with increasing impedance value of the sample.

Table 6. Electrochemical impedance parameters of zinc coating after Cr^{6+} passivation passivation (S1) and Cr-free passivation (S2)

Sample	R_s (Ω cm^2)	R_{pf} (kΩ cm^2)	R_{po} (Ω cm^2)	C_1 (μF cm^{-2})	C_2 (μF cm^{-2})
S1	871.3	130	250	0.223	56
S2	989.2	134	670	0.017	64

The bode diagrams of S1 and S2 during immersion are presented in Fig. 7 a-b. The high frequency region (10^3–10^5 Hz) and the intermediate frequency region (10^0–10^3 Hz) both revealed the capacitive behavior of the passivation film. This behavior indicated the protective effect of the film layer on the galvanized sheet. Furthermore, the impedance measured in the low frequency region (10^{-2}–10 Hz) characterized the electrode response at the interface. Fig. 7 a-b also shows the S1 and S2 phase angle peaks. The phase angle of S2 (85°) was higher than that of S1 (30°), indicating that S2 had a higher corrosion resistance than S1, which is similar to the passivation films corrosion resistance processes reported previously [29].
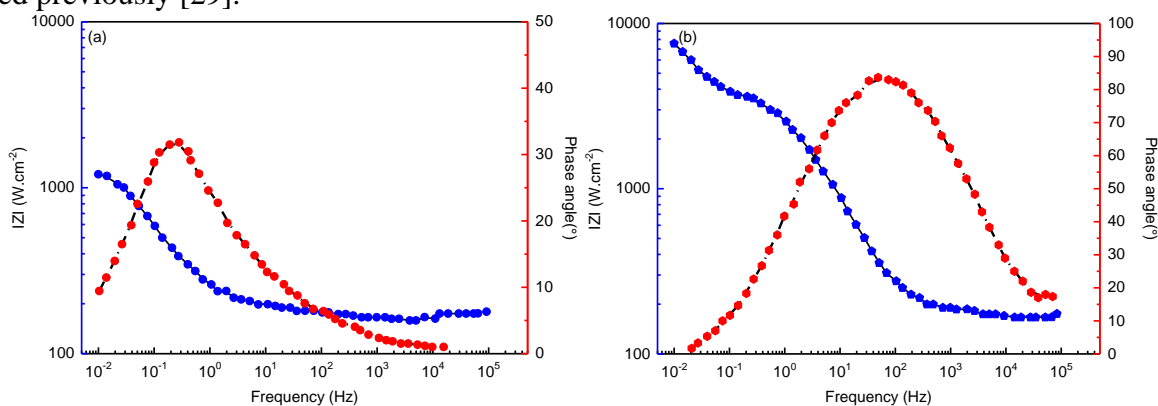

Figure 7. Bode plots of (a) Cr-free passivation films and (b) Cr^{6+} passivation films in 0.5 M NaCl solution.

The corrosion resistance of the Cr-free passivation films prepared in this work was considerably larger than that of other Cr-free passivation films reported in the literature. Table 7 lists the corrosion resistance values of different Cr-free passivation films. The E_{corr} and i_{corr} of the passivator considered in the present work are superior to those of Cr-free passivation films reported in the literature. The results indicated that the Cr-free passivation film prepared by the corresponding surface method has remarkable

corrosion-resistance ability. This ability resulted mainly from the cationic selectivity of the passivation film and the barrier of anions after optimization of the process.

Table 7. Comparison with different methods

Cr-free passivation films	E_{corr} (mV)	j_{corr} (A cm^{-2})
Cr -free passivation on Zn alloys[30]	-1070	0.078
Zn coating after Cr -free passivation[31]	-1100	0.095
Cr -free passivation on nano Zn[32]	-1074	0.114
Trivalent chromium conversion passivate on Zn-Ni alloy[33]	-1180	0.074
Dodecyltrimethylammonium bromide surfactant on zinc electrodes[34]	−1374	0.106
This work	-1031	0.017

4. CONCLUSIONS

(1) The RSM fitting indicated that AD, BC, AC, and BD influenced the corrosion potential, with A, B, C, and D mass ratios of 3.88, 3.53, 3.15, and 1.55 wt.%. The relative deviation between the experimental and theoretical results was 0.12%.

(2) The prepared Cr-free passivation film (average roughness: 0.54–0.90 μm) was free of defects such as zinc particles, zinc bismuth, and scratches. Furthermore, the new Cr-free passivator filled and healed the defected parts of the coating via self-lubrication.

(3) The corrosion resistance performance of the prepared Cr-free passivation film was superior to that of the Cr-containing passivation film. The self-corrosion current densities of S1 and S2 were 0.223 and 0.017 A cm^{-2}, respectively, and the Rct of S2 was 892.6 Ω, which could be effectively reduced. The surface of the galvanized sheet was electronically transmitted to improve the corrosion resistance.

References

1. C.G. Silva, A.N. Correiaa, P.d. Lima-Netoa and O.R. Mattos, *Corros. Sci.*, 47 (2005) 709.
2. T.A. Pozdniakova, L.P. Mazur, R.A.R. Boaventura and V.J.P. Vilar, *J. Clean. Prod.*, 119 (2016) 38.
3. Y.Q. Wang, X. B. Huang and J. Li, *Int. J. Mech. Sci.*, 110 (2016) 201.
4. Q. Li, F. Li and M. An, *J. Mater. Eng. Perform.*, 27 (2018) 3961.
5. Q.Y. Li, H. Lu, J. Cui, M.Z. An and D.Y. Li, *Surf. Coat. Tech.,* 205 (2010) 545.

6. Q. Li, F. Li and M. An, *J. Mater. Eng. Perform.*, 27 (2018) 3961.
7. P.S. Coloma, U. Izagirre, Y. Belaustegi, J.B. Jorcin, F.J. Cano and N. Lapeña, *Appl. Surf. Sci.*, 345 (2015) 24.
8. G. Kong, J.T. Lu, C.S. Che, H.J Wu and S.H. Zhang, *Surf. Coat. Tech.*, 205 (2010) 545.
9. Y.T. Tsai, K.H. Hou, J.L. Lee, M.D. Ger and C.Y. Bai, *Thin Solid Films*, 518 (2010) 7541.
10. B. Lin, J. Lu and G. Kong, *Surf. Coat. Tech.*, 202 (2008) 1831.
11. T.A. Pozdniakova, L.P. Mazur and R.A.R. Boaventura, *Surf. Coat. Tech.*, 119 (2016) 38.
12. B.I. Lin, J.T. LU, G. Kong and L. Jun, *T. Nonferr. Metal. Soc.*, 17 (2007) 755.
13. T.K. Rout and N. Bandyopadhyay, *Anti-Corros. Method. M.*, 54 (2007) 16.
14. H.Y. Su and C.S. Lin, *Corros. Sci.*, 83 (2014) 137.
15. S.M.A. Shibli, B.N. Meena and R. Remya, *Surf. Coat. Tech.,* 262 (2015) 210.
16. Y. Hamlaoui, L. Tifouti and F. Pedraza, *Corros. Sci*., 51 (2009) 2455.
17. K.M. Moon, S.Y. Lee, J.H. Jeong and M.H. Lee, *J. Clean. Prod.*, 119 (2016) 38.
18. K.H. Goh, T.T. Lim and P.C. Chui, *Corros. Sci.*, 50 (2008) 918.
19. L. Francisco, M. Saviano, J.A. Pinto and R. Lourenco, *Curr. Anal. Chem.*, 12 (2016) 256.
20. M. Li, C.P. Feng, Z.Y. Zhang, R.Z. Chen, Q. Xue, C.J. Gao and N. Sugiura, *Electrochim. Acta*, 56 (2010) 265.
21. H. Derikvandi and A. Nezamzadeh, *J. Colloid Interf. Sci.*, 490 (2017) 652.
22. I.H. Cho and K.D. Zoh, *Dyes Pigments*, 75 (2007) 533.
23. M.İ. Coşkun and İ.H. Karahan, *J. Alloy. Compd.*, 745 (2018) 840.
24. Y. Han, Y.Q. Xia, X. Chen, L. Sun, D.Y. Liu and X.Y. Ge, *Anti-Corros. Method. M*., 65 (2018) 131.
25. G.M. Treacy, G.D. Wilcox, and M.O.W. Richardson, *J. Appl. Electrochem.,* 29 (1999), 647.
26. T. Morishita, Y. Soneda and H. Hatori, *Electrochim. Acta.*, 52 (2007) 2478.
27. R.S. Patil, M.D. Uplane and P.S. Patil, *Appl. Surf. Sci.*, 326 (2015) 151.
28. J. Baltrusaitis, B. Mendoza-Sanchez, V. Fernandez, R. Veenstra, N. Dukstienee, A. Roberts and N Fairleyg, *Appl. Surf. Sci.*, 326 (2015) 151.
29. W.A. Badawy, and F.M. Al-Kharafi, *Electrochim. Acta*, 44 (1998) 693.
30. C. Müllera, M. Sarreta, E. Garcíaa and J.A. Ortegab, *J. Electrochem. Soc.*, 151 (2004) C149.
31. Q.Y. Li, H. Lu, J. Cui, M.Z. An, D.Y. Li, *Surf. Coat. Tech.*, 324 (2017) 146.
32. A.K. Guin, M. Bhadu, M. Sinhababu, R.K. Tapan and G. Udayabhanu, *Pigm. Resin. Technol*., 44 (2015) 239.
33. H.H. Sheu, H.B. Lee, S.Y. Jian, C.Y. Hsu, and C.Y. Lee, *Surf. Coat. Tech.*, 305 (2016), 241.
34. K. Liu, P. He, H. Bai, Chen, J.F. Dong, S. Wang, and S. Yuan, *Mater. Chem. Phys.*, 199 (2017), 73.